Journal of Mining and Earth Sciences

Website: https://jmes.humg.edu.vn

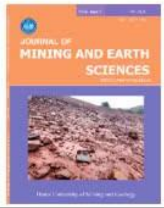

Model-free recursion-based control for 5-degree-of-freedom under-actuated Autonomous Underwater Vehicles via online-tranining neural network

Tung Thanh Sy Ngo [1], Dung Manh Do [2,*], Hai Xuan Le [3], Khoat Duc Nguyen [1]

[1] *Hanoi University of Mining and Geology, Hanoi, Vietnam*
[2] *Hanoi University of Science and Technology, Hanoi, Vietnam*
[3] *Hanoi National University, Hanoi, Vietnam*

ARTICLE INFO

Article history:
Received 28th Nov. 2024
Revised 10th Mar. 2025
Accepted 23rd Mar. 2025

Keywords:
Model-free Control,
Neural Network,
Recursion-based control,
Under-actuated Autonomous,
Underwater Vehicles.

ABSTRACT

The ability to operate in underwater conditions autonomously without human intervention is one of the most intrigued salient features of Autonomous Underwater Vehicles (AUVs), directly leading to profound attention from the scientific community in recent years. However, the scientific research focusing on improving the AUVs' operation is challenged due to the lack of actuators, unknown dynamics, uncertain parameters and strong nonlinearities. To overcome the technical restriction caused by the actuator shortfall, this paper introduces a new control strategy for under-actuated AUVs (UAUVs) with five degrees of freedom, utilising the recursion technique and an artificial neural network. The recursion technique in this paper is designed based on a new modified formula for tracking errors, with a double-loop configuration, resulting in the equivalence to a strictly feedback nonlinear system of under-actuated AUVs. Meanwhile, the neural network used in this paper not only addresses the system's uncertainties but also enhances the controller's adaption. Furthermore, the network's learning rule is implemented online, thereby reducing the computational burden and maintaining the AUVs' stability over the course of the training process. The effectiveness of the controller is verified by sophisticated numerical simulation on Matlab and Simulink platforms. Compared to other existing methods, such as traditional Backstepping control, the proposed method offers a smaller tracking error approximately 20%. The proposed method contributes to the class of control strategies for under-actuated AUVs in a specific speaking and for under-actuated uncertain nonlinear systems in general speaking.

*Corresponding author
E - mail: dung.DM232193M@sis.hust.edu.vn
DOI: 10.46326/JMES.2025.66(2).06

1. Introduction

Under-actuated Autonomous Underwater Vehicles (UAUVs) have consistently garnered significant attention from experts worldwide because of their useful capability of autonomously operating underwater (Fossen, 1999). Thank to this ability, AUVs can support scientists conducting various difficult tasks such as pipeline inspections, underwater environment research, military operations, and resource discoveries (Kim et al., 2015). Despite the unmanned nature of the UAUVs system providing considerable advantages, it also establishes a formidable standard for the autonomous driving system to meet. With several inputs and outputs, strong nonlinearities, and insufficient actuators, the UAUVs are considered a complicated system and challenging to control. Furthermore, a variety of external environmental disturbances and disruptions where UAUVs work, such as hydraulic pressure, waves, and water currents, pose a dramatic difficulty in designing a state-feedback controller for UAUVs. The designed controller must not only drive UAUVs tracking a desired trajectory but also address the uncertain dynamics. Therefore, further studies in the UAUVs are critical.

The number of important techniques dealing with UAUVs' control challenges and applying to different UAUVs have been investigated in various scientific publications. To our best knowledge, the priorities of UAUVs' control studies in recent years include two main topics: nonlinear controller design and artificial intelligence-integrated controller development. For example, Kim et al. (2015) presented the TDC approach. A novel technique for improving the UAUV's locations using a linear controller and time-delay parameter estimation was presented by the authors of (Kim et al., 2015). A non-singular sliding mode control technique for UAUV system tracking problems was presented by Wang et al., (2019). They created a combination of the slow time disturbance observer, backstepping method, and SMC approach (Shen et al., 2016). A different strategy is the active disturbance compensation control, etc., which is suggested by Wang et al. (2019). All methods, however, have some limitations that may negatively affect the well-functional properties of the system like the chattering phenomenon caused by the SMC approach in (Wang et al., 2019; Shen et al., 2016). Even though the saturation function may be used to reduce the effects of this undesired phenomenon, the chattering still deteriorates the actuators' durability. A disturbance compensation technique or disturbance observers must be similar to the precise mathematical model of the system (An et al., 2022; Luo et al., 2023). In general speaking, it can be observed that the principles and techniques mentioned earlier are not typically applicable to systems lacking actuators, including uncertain dynamics and operating in adverse conditions. This is because such systems present unique challenges and complexities that render the conventional maxims ineffective or inapplicable in addressing their specific control requirements.

This study introduces an innovative control strategy grounded in the recursion principle, offering a transformative approach to addressing the challenges of under-actuated autonomous underwater vehicles. The core technique of this method is the redefinition of the tracking error, enabling the complex dynamics of the UAUVs to be reformulated into an equivalent strict feedback nonlinear system. This critical transformation simplifies the system's structure and ensures that the stability of the equivalent model directly translates to the stability of the original 5-DoF U-AUV. The recursion principle, widely recognized for its efficacy in stabilizing strictly feedback nonlinear systems, forms the foundation of this approach. Compared to existing methods (Luo et al., 2023; Kim et al., 2023a), the proposed strategy not only reduces computational complexity but also enhances robustness and reliability in controller design. By leveraging the equivalent model, the 5-DoF UAUV system achieves accurate trajectory tracking within a significantly reduced timeframe, showcasing superior performance. This methodology effectively overcomes the limitations of conventional techniques, providing a streamlined and efficient solution to the under-actuated AUV tracking problem. Its blend of theoretical rigor and practical applicability underscores its potential to advance controller design in this domain.

To deal with the uncertainties of the studied AUV system, all the unknown factors and parameters are combined into a unique vector and estimated by a neural network. A network is designed and integrated into the control scheme with a proposed online rule, calculated from the Lyapunov function. By the by, the neural network is trained simultaneously with the U-AUV's stabilisation process. The compulsory requirement of designing the online training rule is that it is not allowed to affect the stability of the U-AUV. As a result, when the neural network is converged, the states of the U-AUV are also stabilised at the desired value. The performance of reducing the computational burden of this paper's proposed scheme is more effective than the offline training rule in (Song et al., 2019). Moreover, the cooperation between the recursion-based controller and the neural network is called the model-free recursion-based control because of releases the dependence on the mathematical model. This is the main our proposal. The proposed method contributes to the class of control strategies for under-actuated AUVs in specific speaking and for under-actuated uncertain nonlinear system in general speaking.

This paper is structured as follows: Section 2 presents the mathematical model of the system, as well as the control objectives. Section 3 outlines the step-by-step design process of both the kinematic and dynamic controller to address the UAUV tracking problem. The neural network is also designed here. Section 4 presents all simulation results, followed by the conclusion in the subsequent sections.

2. System Information and Control objectives

2.1. Mathematical Model

Considering the 5-Dof U-AUV system studied in the article (Tung et al., 2023), the motion of the U-AUV is illustrated in Figure 1 through two coordinate systems: the Earth-Fixed Frame, the so-called NED system, and the Body-Fixed Frame. x, y, z are three states determining the positions of the studied system in the NED frame and θ, ψ are two states representing the U-AUV's rotation angles. In this paper, x, y, z and θ, ψ are combined into a unique vector $\boldsymbol{\eta} = [x \quad y \quad z \quad \theta \quad \psi]^T$ to easily design a model-free controller. The first-

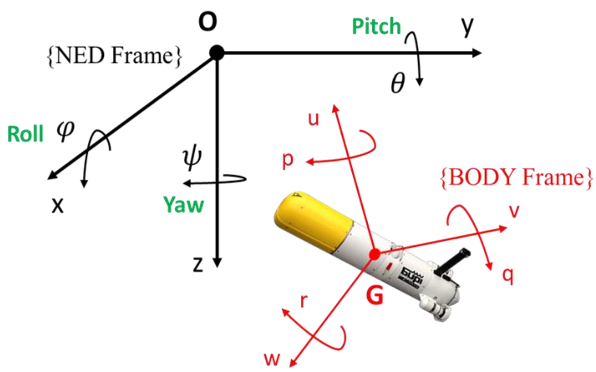

Figure 1. The motion of the U-AUV.

order derivative $\dot{\boldsymbol{\eta}} = [\dot{x} \quad \dot{y} \quad \dot{z} \quad \dot{\theta} \quad \dot{\psi}]^T$ symbolises the velocities in the NED frame. In the BODY frame, a vector of UAUV's velocities is symbolised by $\boldsymbol{v}$ and it is calculated by $\boldsymbol{v} = [u \quad v \quad w \quad q \quad r]^T$. Relationship between $\dot{\boldsymbol{\eta}}$ and $\boldsymbol{v}$ is represented by a kinematic equation (Fossen, 1999):

$$\dot{\boldsymbol{\eta}} = \boldsymbol{J}(\boldsymbol{\eta})\boldsymbol{v} \tag{1}$$

In which $\boldsymbol{J}(\boldsymbol{\eta}) = \mathrm{diag}\big(\boldsymbol{J_1}(\boldsymbol{\eta}), \boldsymbol{J_2}(\boldsymbol{\eta})\big)$ is the Jacobian matrix with $\boldsymbol{J_1}(\boldsymbol{\eta}) \in \mathbb{R}^{3\times3}$ and $\boldsymbol{J_2}(\boldsymbol{\eta}) \in \mathbb{R}^{2\times2}$. Both $\boldsymbol{J_1}(\boldsymbol{\eta})$ and $\boldsymbol{J_2}(\boldsymbol{\eta})$ are detailedly calculated in the paper (Wang et al., 2019). Denote $\boldsymbol{\tau} = [\tau_u \quad 0 \quad 0 \quad \tau_q \quad \tau_r]^T$ as a vector of input signals. The dynamic model of the U-AUV can be expressed as follows (Fossen, 1999).

$$\boldsymbol{M}\dot{\boldsymbol{v}} + \boldsymbol{C}(\boldsymbol{\eta}, \dot{\boldsymbol{\eta}}, \boldsymbol{\gamma})\boldsymbol{v} + \boldsymbol{G}(\boldsymbol{\eta}, \boldsymbol{\gamma}) = \boldsymbol{\tau} + \boldsymbol{d} \tag{2}$$

Where $\boldsymbol{M} \in \mathbb{R}^{5\times5}$ is the matrix of inner masses. $\boldsymbol{C}(\boldsymbol{\eta}, \dot{\boldsymbol{\eta}}, \boldsymbol{\gamma}) \in \mathbb{R}^{5\times5}$ is the matrix of all Coriolis and buoyancy factors. $\boldsymbol{G}(\boldsymbol{\eta}, \boldsymbol{\gamma})$ and $\boldsymbol{d}$ are the vectors of gravity and external disturbances, respectively. $\boldsymbol{\gamma}$ represents all unknown and uncertain factors. Matrices $\boldsymbol{M}$, $\boldsymbol{C}(\boldsymbol{\eta}, \dot{\boldsymbol{\eta}}, \boldsymbol{\gamma})$ and $\boldsymbol{G}(\boldsymbol{\eta}, \boldsymbol{\gamma})$ are calculated in (Chen et al., 2023). By symbolising $\boldsymbol{\tau_a} = [\tau_u \quad \tau_q \quad \tau_r]^T$, the dynamic model (2) can be separated into two subsystems. One is the system of fully actuated states $\boldsymbol{v_a} = [u \quad q \quad r]^T$ and another is the system of under-actuated states $\boldsymbol{v_u} = [v \quad w]^T$. They are represented as the following:

$$\boldsymbol{M_a}\dot{\boldsymbol{v}}_{\boldsymbol{a}} + \boldsymbol{C_a}(\boldsymbol{\eta}, \dot{\boldsymbol{\eta}}, \boldsymbol{\gamma})\boldsymbol{v_a} + \boldsymbol{G_a}(\boldsymbol{\eta}, \boldsymbol{\gamma}) = \boldsymbol{\tau_a} \tag{3}$$

$$\boldsymbol{M_u}\dot{\boldsymbol{v}}_{\boldsymbol{u}} + \boldsymbol{C_u}(\boldsymbol{v}, \boldsymbol{\gamma})\boldsymbol{v_u} + \boldsymbol{G_u}(\boldsymbol{\eta}, \boldsymbol{\gamma}) = \boldsymbol{0} \tag{4}$$

In which $\boldsymbol{M_{a,u}}$, $\boldsymbol{C_{a,u}}(\boldsymbol{\eta}, \dot{\boldsymbol{\eta}}, \boldsymbol{\gamma})$ and $\boldsymbol{G_{a,u}}(\boldsymbol{\eta}, \boldsymbol{\gamma})$ are computed in (Chen et al., 2023). The under-actuated subsystem (4) is weekly stable because the negative-define property of the matrix $\boldsymbol{M}_u^{-1}\boldsymbol{C}_{\boldsymbol{u}}(\boldsymbol{v},\boldsymbol{\gamma}) = \mathrm{diag}(|\gamma_1|m_1, |\gamma_2|m_2)$ with $m_1 = \frac{Y_{vv}|v|+Y_v}{M-Y_{\dot{v}}} < 0$, $m_2 = \frac{Z_{ww}|w|+Z_w}{M-Y_{\dot{v}}} < 0$ and vector $\boldsymbol{M}_u^{-1}\boldsymbol{G}_{\boldsymbol{u}}(\boldsymbol{\eta},\boldsymbol{\gamma})$ is bounded according to (Qiao and Zhang, 2018). Therefore, if the fully actuated system (3) achieves stability, system (2) will also be stable within the vicinity of the origin.

Assumption 1 (Qiao and Zhang, 2018)***:*** Angle θ satisfies:

$$-\frac{\pi}{2} < \theta < \frac{\pi}{2} \tag{5}$$

Lemma 2 (Tung et al., 2023; Shen et al., 2016)***:*** $\boldsymbol{J_1}(\boldsymbol{\eta})$is an orthogonal matrix and it is satisfied:

$$\boldsymbol{J}_1^T(\boldsymbol{\eta})\dot{\boldsymbol{J}}_1(\boldsymbol{\eta}) = \boldsymbol{\Xi} \tag{6}$$

$$\boldsymbol{J}_1^T(\boldsymbol{\eta}) = \boldsymbol{J}_1^{-1}(\boldsymbol{\eta}) \tag{7}$$

Where $\boldsymbol{\Xi} = \begin{bmatrix} 0 & -r & q \\ r & 0 & r\tan\theta \\ -q & -r\tan\theta & 0 \end{bmatrix}$. Matrix $\boldsymbol{\Xi}$makes $\boldsymbol{x^T\Xi x} = \boldsymbol{0}$, $\forall \boldsymbol{x} \in \mathbb{R}^3$. Because the matrix $\boldsymbol{\Xi}$is a skew-symmetric matrix, the equation is held:

$$\boldsymbol{\Xi} + \boldsymbol{\Xi}^T = \boldsymbol{\Theta}_3 \tag{8}$$

Remark 1. The under-actuated AUV studied in the previous paper (Chen et al., 2023) is assumed to be exact and all its parameters are known. However, this assumption in reality is quite difficult to achieve because parameters can be changed during the AUV's operation. The under-actuated AUV studied here, with the presence of unknown factors $\boldsymbol{\gamma}$, is more general than the system in (Chen et al., 2023)

Remark 2. Although $\boldsymbol{J_1}(\boldsymbol{\eta})$is an orthogonal matrix, $\boldsymbol{J}_2(\boldsymbol{\eta})$ is not. Thus, $\boldsymbol{J}^T(\boldsymbol{\eta}) \neq \boldsymbol{J}^{-1}(\boldsymbol{\eta})$.

2.2. AUV operation's environmental conditions

The main types of disturbances affecting AUVs include currents, waves, and water pressure. Currents affect the input moments of the vehicle through the damping matrix. Meanwhile, water pressure and ocean waves are considered matching-type disturbances, which impact the AUV through the hull and directly influence the input force signal τ. Therefore, a stacking method is used to approximate the effects of waves, currents, and water pressure.

2.2.1. Ocean flow

The ocean currents, referred to as deep-water currents, are large-scale water flows that move at great depths in the ocean. These currents can directly affect the hull of the vehicle, influencing its course. Specifically, at greater depths, water pressure increases due to the weight of the water above, creating an external pressure on the hull. Therefore, the hull must be designed to withstand this pressure to avoid damage and leakage. Additionally, horizontal currents may appear at sufficient depths, generating resistance to the vehicle when moving through them, which affects its performance and requires adjustments during navigation. Moreover, factors such as temperature, salinity, and sound also influence the stability of the vehicle's movement and require control measures. However, these factors tend to change slowly (Fossen, 1999). In this paper, it is assumed that the changes in current are negligible when dealing with control applications for AUVs operating at low speeds.

2.2.2. Ocean wave

Ocean waves can affect AUVs in various ways, including water oscillation, wave propagation, sound, drag, and resistance. Specifically, ocean waves create water oscillations, and depending on the size and characteristics of the waves, the AUV may encounter water fluctuations. This can make it challenging to maintain the stability of the vehicle, particularly when operating at shallow depths and near the ocean surface.

2.2.3. Hydraulic pressure

Water pressure plays a significant role for AUVs, especially when they dive deep into the ocean. The impact of water pressure on the vehicle can be viewed from several angles: increased pressure, material elasticity, movement in the water, and travel speed. Specifically, the water pressure increases with depth, creating an external force on the hull. This pressure can become substantial, so the vehicle must be constructed to withstand high pressure. Analyzing the impact of water pressure on the vehicle is relatively complex because, according to Pascal's principle, water pressure affects the AUV in all directions. However, the vertical pressure effect is the strongest due to the large mass of water above the AUV. In this study, it is assumed that the water pressure at a specific depth remains constant and is directly added to the control signal, serving as the mismatched disturbances of the U-AUVs.

2.3. Control Objectives

There are two control objectives in this paper listed as follows:

- Develop a new model-free recursion principle-based control for the 5-Dof under-actuated AUV system under the conditions of unknown factors and external disturbances. The proposed controller must be independent of the U-AUV's mathematical model to ensure the control performance in the case of the changed parameters.

- Design an online training rule for the utilised neural network to update the parameters of the proposed controller and make the closed-loop system stable. Additionally, online training for the neural network helps to reduce the computational burden compared to offline training.

3. Main design

3.1. Recursion-based Controller Design

In this section, the procedure of the recursion-based controller design is presented step-by-step for easy readability. The proposed control strategy is designed with double-loop scheme. First, denote $\boldsymbol{\eta_{1d}} = [x_d \quad y_d \quad z_d]^T$ is the vector of the desired U-AUV's position. One of the key techniques in this paper is a new transformation to tracking errors. Hence, it helps to find a new equivalent model of the 5-Dof U-AUV as a strictly feedback nonlinear system. As a result, the stability of the equivalent model leads to the stability of the 5-Dof U-AUV model.

Step 1: Define a new diffeomorphis for tracking errors.

A vector of new tracking error is noted by $\boldsymbol{s_1}$. It is calculated by the following:

$$\boldsymbol{s_1} = \boldsymbol{\xi_1} - \boldsymbol{\delta} - \boldsymbol{J_1^T}(\boldsymbol{\eta})\boldsymbol{\dot{e}_1} \tag{9}$$

$$\boldsymbol{\xi_1} = \boldsymbol{J_1^T}(\boldsymbol{\eta})\big(\boldsymbol{\dot{e}_1} + \boldsymbol{A}\boldsymbol{e_1} + \boldsymbol{J_1}(\boldsymbol{\eta})\boldsymbol{\delta}(t)\big) \tag{10}$$

$$\boldsymbol{e_1} = \begin{pmatrix} (\boldsymbol{\dot{\eta}_1} - \boldsymbol{\dot{\eta}_{1d}}) + \lambda_1(\boldsymbol{\eta_1} - \boldsymbol{\eta_{1d}}) \\ +\lambda_2|\boldsymbol{\eta_1} - \boldsymbol{\eta_{1d}}|^{\beta} sig(\boldsymbol{\eta_1} - \boldsymbol{\eta_{1d}}) \end{pmatrix} \tag{11}$$

Where $\boldsymbol{\delta}(t) = [\delta(t) \quad 0]^T$ is the time-varying vector of exploration noise, $\delta(t)$is an arbitrary noise function satisfying $\delta(t) > 0$for all t. $\lambda_1 > \lambda_2 > 0$, $\boldsymbol{A}$ is an arbitrarily positive-define matrix and the exponential term βsatisfying $0 < \beta < 1$.

From equation (10), obviously, $\boldsymbol{s_1} \to \boldsymbol{0}$ by the proposed controller, it will achieve $\boldsymbol{\xi_1} \to \boldsymbol{\delta} + \boldsymbol{J_1^T}(\boldsymbol{\eta})\boldsymbol{\dot{e}_1}$. By using equation (6) and a positive-define matrix $\boldsymbol{A}$, we have $\boldsymbol{e_1} \to 0$. The under-actuated UAUV system follows the desired trajectory according to **Lemma 1**. This task is for a kinematic and dynamic controller designed in the next steps.

Step 2: Transformation to the equivalent model

To steer $\boldsymbol{s_1} \to \boldsymbol{0}$, the step-by-step process will be demonstrated in the design procedure, including the calculation of the derivative of $\boldsymbol{s_1}$. Derivation from both sides of equation (5) yields:

$$\begin{aligned} \boldsymbol{\dot{s}_1} &= \boldsymbol{\dot{\xi}_1} - \boldsymbol{\dot{\delta}} - \boldsymbol{\dot{J}_1^T}(\boldsymbol{\eta})\boldsymbol{\dot{e}_1} - \boldsymbol{J_1^T}(\boldsymbol{\eta})\boldsymbol{\ddot{e}_1} \\ &= \boldsymbol{\dot{J}_1^T}(\boldsymbol{\eta})\boldsymbol{A}\boldsymbol{e_1} + \boldsymbol{J_1^T}(\boldsymbol{\eta})\boldsymbol{A}\boldsymbol{\dot{e}_1} \end{aligned} \tag{12}$$

From equations (1), (9), (10) and (11), yields:

$$\boldsymbol{\dot{\eta}}_1 = \boldsymbol{J_1}(\boldsymbol{\eta})\boldsymbol{v_1} \tag{13}$$

$$\boldsymbol{e_1} = \boldsymbol{A}^{-1}\boldsymbol{J_1}(\boldsymbol{\eta})\boldsymbol{s_1} \tag{14}$$

$$\boldsymbol{\dot{e}_1} = \lambda_1(\boldsymbol{\dot{\eta}_1} - \boldsymbol{\dot{\eta}_{1d}}) + \boldsymbol{f} \tag{15}$$

$$\begin{aligned} \boldsymbol{f} = \big[\boldsymbol{\ddot{\varsigma}_1} + |\boldsymbol{\varsigma_1}|^{\beta-1}\big(\lambda_2\beta \\ + \lambda_2|\boldsymbol{\varsigma_1}|D(\boldsymbol{\varsigma_1})\big)\big] \end{aligned} \tag{16}$$

Where $\boldsymbol{\varsigma_1} = \boldsymbol{\eta_1} - \boldsymbol{\eta_{1d}}$ and $\boldsymbol{v_1} = [u \quad v \quad w]^T$. $D(\boldsymbol{\varsigma_1}) = \begin{cases} +\infty, & \boldsymbol{\varsigma_1} = 0 \\ 0, & \boldsymbol{\varsigma_1} \neq 0 \end{cases}$ is a dirac delta impulse function of $\boldsymbol{\varsigma_1}$. Substituting (13), (14), (15) into equation (12) we have:

$$\boldsymbol{\dot{s}_1} = \begin{bmatrix} \boldsymbol{\dot{J}_1^T}(\boldsymbol{\eta})\boldsymbol{J_1}(\boldsymbol{\eta})\boldsymbol{s_1} + \boldsymbol{J_1^T}(\boldsymbol{\eta})\boldsymbol{A}\boldsymbol{f} \\ +\lambda_1\boldsymbol{J_1^T}(\boldsymbol{\eta})\boldsymbol{A}(\boldsymbol{J_1}(\boldsymbol{\eta})\boldsymbol{v_1} - \boldsymbol{\dot{\eta}_{1d}}) \end{bmatrix} \tag{17}$$

Using the equation (6), it can deduce that:

$$\begin{aligned} &\varXi + \varXi^T = (\varXi + \varXi^T)\boldsymbol{\delta} \\ &= \lambda_1 \boldsymbol{J}_1^T(\boldsymbol{\eta})\boldsymbol{A}\boldsymbol{J}_1(\boldsymbol{\eta})(\varXi + \varXi^T)\boldsymbol{\delta} = \boldsymbol{\Theta}_3 \end{aligned} \tag{18}$$

From (12) and (17), (18) we have:

$$\dot{\boldsymbol{s}}_1 = \begin{bmatrix} \varXi^T \boldsymbol{s}_1 + \boldsymbol{J}_1^T(\boldsymbol{\eta})\boldsymbol{A}\boldsymbol{f} \\ +\lambda_1 \boldsymbol{J}_1^T(\boldsymbol{\eta})\boldsymbol{A}\boldsymbol{J}_1(\boldsymbol{\eta})(\boldsymbol{v}_1 + \varXi^T\boldsymbol{\delta}) \\ -\lambda_1 \boldsymbol{J}_1^T(\boldsymbol{\eta})\boldsymbol{A}\dot{\boldsymbol{\eta}}_{1d} \\ +\lambda_1 \boldsymbol{J}_1^T(\boldsymbol{\eta})\boldsymbol{A}\boldsymbol{J}_1(\boldsymbol{\eta})\varXi\boldsymbol{\delta} \end{bmatrix} \tag{19}$$

According to Chen et al. (2023), the below equation is held:

$$\boldsymbol{v}_1 + \varXi^T\boldsymbol{\delta} = (\boldsymbol{E}_3 + \boldsymbol{\Phi})\boldsymbol{v}_a + \boldsymbol{\mu} \tag{20}$$

Where the matrix $\boldsymbol{\Phi} = \begin{bmatrix} 0 & 0 & 0 \\ 0 & -1 & -\delta \\ 0 & \delta & -1 \end{bmatrix}$ and the vector $\boldsymbol{\mu} = [0 \quad v \quad w]^T$. Because of the positive function $\delta(t)$, matrix $(\boldsymbol{E}_3 + \boldsymbol{\Phi})$is always invertible. From equations (19) and (20), the model of tracking error is determined by:

$$\dot{\boldsymbol{s}}_1 = \begin{bmatrix} \varXi^T \boldsymbol{s}_1 + \boldsymbol{J}_1^T(\boldsymbol{\eta})\boldsymbol{A}(\boldsymbol{f} + \lambda_1 \boldsymbol{J}_1 \varXi\boldsymbol{\delta}) \\ +\lambda_1 \boldsymbol{J}_1^T \boldsymbol{A}(\boldsymbol{J}_1(\boldsymbol{\eta})\boldsymbol{\mu} - \lambda_1 \dot{\boldsymbol{\eta}}_{1d}) \\ +\lambda_1 \boldsymbol{J}_1^T \boldsymbol{A}\boldsymbol{J}_1(\boldsymbol{\eta})(\boldsymbol{E}_3 + \boldsymbol{\Phi})\boldsymbol{v}_a \end{bmatrix} \tag{21}$$

Finally, using equations (3) and (4), the equivalent model of 5-Dof U-AUV with the tracking error vector $\boldsymbol{s}_1$ as states is represented by the following:

$$\begin{cases} \dot{\boldsymbol{s}}_1 = \begin{pmatrix} \varXi^T \boldsymbol{s}_1 + \boldsymbol{\lambda}_z(\boldsymbol{\eta}, \boldsymbol{v}) \\ +\lambda_1 \boldsymbol{J}_1^T \boldsymbol{A}\boldsymbol{J}_1(\boldsymbol{E}_3 + \boldsymbol{\Phi})\boldsymbol{v}_a \end{pmatrix} \\ \dot{\boldsymbol{v}}_a = \boldsymbol{M}_a^{-1}\boldsymbol{\tau}_a + \boldsymbol{\lambda}(\boldsymbol{v}_a, \boldsymbol{\eta}, \boldsymbol{\gamma}) \end{cases} \tag{22}$$

Where:

$$\boldsymbol{\lambda}_z(\boldsymbol{\eta}, \boldsymbol{v}) = \boldsymbol{J}_1^T(\boldsymbol{\eta})\boldsymbol{A}\phi(\boldsymbol{\eta}, \boldsymbol{v}) \tag{23}$$

$$\phi(\boldsymbol{\eta}, \boldsymbol{v}) = \begin{pmatrix} \lambda_1 \boldsymbol{J}_1(\boldsymbol{\eta})\varXi\boldsymbol{\delta} - \lambda_1 \dot{\boldsymbol{\eta}}_{1d} \\ +\lambda_1 \boldsymbol{J}_1(\boldsymbol{\eta})\boldsymbol{\mu} + \boldsymbol{f}(\boldsymbol{\varsigma}_1) \end{pmatrix} \tag{24}$$

$$\boldsymbol{\lambda}(\boldsymbol{v}_a, \boldsymbol{\eta}, \boldsymbol{\gamma}) = \begin{bmatrix} \boldsymbol{M}_a^{-1}\boldsymbol{C}_a(\boldsymbol{\eta}, \dot{\boldsymbol{\eta}}, \boldsymbol{\gamma})\boldsymbol{v}_a \\ +\boldsymbol{M}_a^{-1}\boldsymbol{G}_a(\boldsymbol{\eta}, \boldsymbol{\gamma}) \end{bmatrix} \tag{25}$$

Obviously, system (22) constitutes a strict feedback nonlinear system, with the vector $\boldsymbol{v}_a$ being interpreted as a

virtual input signal. Thanks to the new transformation to the tracking error (9)-(11), the under-actuation factors of the 5-Dof U-AUV system in position problem are eradicated. The next step's mission is to design $\boldsymbol{\tau}_a$in such a way that $\boldsymbol{s}_1 \to \boldsymbol{0} \Leftrightarrow \boldsymbol{\eta}_1 \to \boldsymbol{\eta}_{1d}$.

Remark 3. On account of the orthogonal matrix$\boldsymbol{J}_1(\boldsymbol{\eta})$, matrices $\boldsymbol{J}_1^T(\boldsymbol{\eta})\boldsymbol{A}\boldsymbol{J}_1(\boldsymbol{\eta})$ and $\boldsymbol{A}$ are similar. Because $\boldsymbol{A}$ is a positive-define matrix, $\boldsymbol{J}_1^T(\boldsymbol{\eta})\boldsymbol{A}\boldsymbol{J}_1(\boldsymbol{\eta})$ is also a positive-define matrix. It; therefore, is invertible.

Step 3: Kinematic Controller Design

The aim of this step is to determine $\boldsymbol{v}_a$to steer $\boldsymbol{s}_1 \to \boldsymbol{0}$. To do this, we set:

$$\boldsymbol{v}_a = \boldsymbol{v}_{ad} + \boldsymbol{z}_1 \tag{26}$$

Substituting (26) into the equation (22) yields:

$$\dot{\boldsymbol{s}}_1 = \begin{pmatrix} \lambda_1 \boldsymbol{J}_1^T(\boldsymbol{\eta})\boldsymbol{A}\boldsymbol{J}_1(\boldsymbol{E}_3 + \boldsymbol{\Phi})\boldsymbol{z}_1 \\ +\lambda_1 \boldsymbol{J}_1^T(\boldsymbol{\eta})\boldsymbol{A}\boldsymbol{J}_1(\boldsymbol{E}_3 + \boldsymbol{\Phi})\boldsymbol{v}_{ad} \\ +\boldsymbol{\lambda}_z(\boldsymbol{\eta}, \boldsymbol{v}) + \varXi^T \boldsymbol{s}_1 \end{pmatrix} \tag{27}$$

As can be seen from (27), $\boldsymbol{\lambda}_z(\boldsymbol{\eta}, \boldsymbol{v})$ is unknown due to the impracticable function $D(\boldsymbol{\varsigma}_1)$. Therefore, to make $\boldsymbol{s}_1 \to \boldsymbol{0}$, using a candidate Lyapunov function:

$$V_1(\boldsymbol{s}_1) = \frac{1}{2}\boldsymbol{s}_1^T \boldsymbol{P} \boldsymbol{s}_1 + \frac{1}{2}\tilde{\boldsymbol{\lambda}}_z^T \boldsymbol{\Phi}^{-1} \tilde{\boldsymbol{\lambda}}_z \tag{28}$$

Where $\tilde{\boldsymbol{\lambda}}_z = \boldsymbol{\lambda}_z(\boldsymbol{\eta}, \boldsymbol{v}) - \hat{\boldsymbol{\lambda}}_z$ and $\hat{\boldsymbol{\lambda}}_z$is the estimated vector of $\boldsymbol{\lambda}_z(\boldsymbol{\eta}, \boldsymbol{v})$. $\boldsymbol{P}, \boldsymbol{\Phi}$ is two positive-define matrices. Differentiating from both sides of equation (28) and using (27) yields:

$$\begin{aligned} &\dot{V}_1 \\ &= \boldsymbol{s}_1^T \boldsymbol{P} \begin{pmatrix} \lambda_1 \boldsymbol{J}_1^T(\boldsymbol{\eta})\boldsymbol{A}\boldsymbol{J}_1(\boldsymbol{E}_3 + \boldsymbol{\Phi})\boldsymbol{z}_1 \\ -\boldsymbol{K}_1 \tanh(\boldsymbol{s}_1) - \boldsymbol{K}_2 |\boldsymbol{s}_1|^{2\beta-1} \end{pmatrix} \\ &+ \tilde{\boldsymbol{\lambda}}_z^T \boldsymbol{\Phi}^{-1} \alpha_1 (\boldsymbol{\lambda}_z(\boldsymbol{\eta}, \boldsymbol{v}) - \tilde{\boldsymbol{\lambda}}_z) \end{aligned} \tag{29}$$

$$\begin{aligned} &\dot{V}_1 \le \\ &\boldsymbol{s}_1^T \boldsymbol{P} \begin{pmatrix} \lambda_1 \boldsymbol{J}_1^T(\boldsymbol{\eta})\boldsymbol{A}\boldsymbol{J}_1(\boldsymbol{E}_3 + \boldsymbol{\Phi})\boldsymbol{z}_1 \\ -\boldsymbol{K}_1 \tanh(\boldsymbol{s}_1) - \boldsymbol{K}_2 |\boldsymbol{s}_1|^{2\beta-1} \end{pmatrix} + \\ &\alpha_1 \lambda_{max}^{\boldsymbol{\Phi}^{-1}} \|\boldsymbol{\lambda}_z\|_F \|\tilde{\boldsymbol{\lambda}}_z\|_F - \alpha_1 \lambda_{max}^{\boldsymbol{\Phi}^{-1}} \|\tilde{\boldsymbol{\lambda}}_z\|_F^2 \end{aligned} \tag{30}$$

Equation (30) is achieved if and only if:

$$\begin{aligned} &\boldsymbol{v}_{ad} \\ &= -\frac{1}{\lambda_1} \begin{bmatrix} (\boldsymbol{E}_3 + \boldsymbol{\Phi})^{-1} \boldsymbol{J}_1^T \boldsymbol{A}^{-1} \boldsymbol{J}_1(\boldsymbol{\eta}) \times \\ \times \begin{pmatrix} \hat{\boldsymbol{\lambda}}_z + \varXi^T \boldsymbol{s}_1 + \boldsymbol{K}_2 |\boldsymbol{s}_1|^{2\beta-1} \\ +\boldsymbol{K}_1 \tanh(\boldsymbol{s}_1) \end{pmatrix} \end{bmatrix} \end{aligned} \tag{31}$$

$$\dot{\hat{\boldsymbol{\lambda}}}_z = \boldsymbol{\Phi} \boldsymbol{P}^T \boldsymbol{s}_1 - \alpha_1 \hat{\boldsymbol{\lambda}}_z \tag{32}$$

Where $\boldsymbol{K_1}, \boldsymbol{K_2}$ are two positive-define matrices which can be chosen arbitrarily. $\lambda_{max}^{\boldsymbol{\Phi}^{-1}}$ is the largest eigenvalue of the matrix $\boldsymbol{\Phi}^{-1}$. α_1 is a positive small number. From equation (29), if we have $\boldsymbol{z_1} \to 0$, the negative-define property of the first-order derivative of the Lyapunov function $\dot{V}_1$can be achieved. Therefore, the aim of the next step is to make $\boldsymbol{z_1} \to 0$. The convergence velocity depends on the matrix $\boldsymbol{K}_1$.

Step 4: Dynamic Controller Design

To make $\boldsymbol{z_1} \to 0$, using the second candidate Lyapunov function:

$$V_2 = V_1(\boldsymbol{s_1}) + \frac{1}{2}\boldsymbol{z}_1^T \boldsymbol{z_1} \tag{33}$$

Differentiating from both sides of equation (33) yields:

$$\dot{V}_2 = \dot{V}_1(\boldsymbol{s_1}) + \boldsymbol{z}_1^T(\dot{\boldsymbol{v}}_{\boldsymbol{a}} - \dot{\boldsymbol{v}}_{\boldsymbol{ad}}) \tag{34}$$

Substituting equations (22), (30) into (34) gives:

$$\dot{V}_2 \leq \begin{pmatrix} \boldsymbol{\rho}(\boldsymbol{s_1}) + \alpha_1 \lambda_{max}^{\boldsymbol{\Phi}^{-1}} \|\boldsymbol{\lambda_z}\|_F \|\tilde{\boldsymbol{\lambda}}_{\boldsymbol{z}}\|_F \\ +\boldsymbol{z}_1^T \begin{pmatrix} \boldsymbol{M}_a^{-1}\boldsymbol{\tau_a} + \boldsymbol{\lambda}(\boldsymbol{v_a}, \boldsymbol{\eta}, \boldsymbol{\gamma}) - \dot{\boldsymbol{v}}_{\boldsymbol{ad}} \\ +\lambda_1(\boldsymbol{E}_3 + \boldsymbol{\Phi})^T \boldsymbol{J}_1^T \boldsymbol{A}^T \boldsymbol{J_1} \boldsymbol{P}^T \boldsymbol{s_1} \\ +\boldsymbol{K_1}\, tan(\boldsymbol{z}_1) + \boldsymbol{K_2}|\boldsymbol{z}_1|^{2\beta-1} \end{pmatrix} \\ -\boldsymbol{K_1}|\boldsymbol{z}_1| - \boldsymbol{z}_1^T \boldsymbol{K_2}|\boldsymbol{z}_1|^{2\beta-1} \end{pmatrix} \tag{35}$$

$$\dot{V}_2 \leq \begin{pmatrix} \boldsymbol{\rho}(\boldsymbol{s_1}) + \alpha_1 \lambda_{max}^{\boldsymbol{\Phi}^{-1}} \|\boldsymbol{\lambda_z}\|_F \|\tilde{\boldsymbol{\lambda}}_{\boldsymbol{z}}\|_F \\ -\boldsymbol{K_1}|\boldsymbol{z}_1| - \boldsymbol{z}_1^T \boldsymbol{K_2}|\boldsymbol{z}_1|^{2\beta-1} \end{pmatrix}$$

If and only if:

$$\boldsymbol{f_a} = \begin{pmatrix} \boldsymbol{\lambda}(\boldsymbol{v_a}, \boldsymbol{\eta}, \boldsymbol{\gamma}) - \dot{\boldsymbol{v}}_{\boldsymbol{ad}} \\ +\lambda_1(\boldsymbol{E}_3 + \boldsymbol{\Phi})^T \boldsymbol{J}_1^T \boldsymbol{A}^T \boldsymbol{J_1} \boldsymbol{P}^T \boldsymbol{s_1} \\ +\boldsymbol{K_1}\, tanh(\boldsymbol{z}_1) + \boldsymbol{K_2}|\boldsymbol{z}_1|^{2\beta-1} \end{pmatrix} \tag{36}$$

$$\boldsymbol{\tau_a} = -\boldsymbol{M}_a \boldsymbol{f_a}$$

In (35), $\boldsymbol{\rho}(\boldsymbol{s_1}) < 0$ and calculated by:

$$\boldsymbol{\rho}(\boldsymbol{s_1}) = \begin{pmatrix} -\boldsymbol{s}_1^T \boldsymbol{P}\boldsymbol{K_1}\, tanh(\boldsymbol{s}_1) - \\ -\boldsymbol{s}_1^T \boldsymbol{P}\boldsymbol{K_2}|\boldsymbol{s_1}|^{2\beta-1} - \alpha_1 \lambda_{max}^{\boldsymbol{\Phi}^{-1}} \|\tilde{\boldsymbol{\lambda}}_{\boldsymbol{z}}\|_F^2 \end{pmatrix}$$

Remark 4. It is necessary to choose the gain matrix $\boldsymbol{\Phi}$being large enough. It results in the small value of $\lambda_{max}^{\boldsymbol{\Phi}^{-1}}$. By selecting $\boldsymbol{K_1}$ and $\boldsymbol{K_2}$to be large enough, the negative property of $\dot{V}_2$is maintain. Thus, the recursion-based controller brings the bounded stability for the U-AUV's closed-loop system.

3.2. Model-free Controller Design

For the sake of including the unknown factors $\boldsymbol{\gamma}$, controller (36) is impracticable. To deal with this problem, this paper proposes a new model-free controller by replacing $\boldsymbol{\lambda}(\boldsymbol{v_a}, \boldsymbol{\eta}, \boldsymbol{\gamma})$ by its estimation $\hat{\boldsymbol{\lambda}}(\boldsymbol{v_a}, \boldsymbol{\eta})$. $\hat{\boldsymbol{\lambda}}(\boldsymbol{v_a}, \boldsymbol{\eta})$ is computed by a neural network with three layers and its matrix of weights is symbolised by $\Re \in \mathbb{R}^{3\times N}$. $N$is the number of neurons in the hidden layer. $\Re$is assumed to satisfy the boundedness $\|\Re\|_F < +\infty$. The designed neural network has $\boldsymbol{v_a}, \boldsymbol{\eta}$as its input signals and its output is determined by the following (Yang et al., 2018):

$$\boldsymbol{\lambda}(\boldsymbol{v_a}, \boldsymbol{\eta}, \boldsymbol{\gamma}) = \Re^T \omega(\boldsymbol{v_a}, \boldsymbol{\eta}) + \zeta \tag{37}$$

Where $\zeta$is the estimated error of the used neural network. $\omega(\boldsymbol{v_a}, \boldsymbol{\eta}) = col\big(\omega_i(\boldsymbol{v_a}, \boldsymbol{\eta})\big)$ with $i = 1,2,\ldots,N$ is the activation function calculated by:

$$\omega_i(\boldsymbol{v_a}, \boldsymbol{\eta}) = \frac{\sigma_i(\boldsymbol{v_a}, \boldsymbol{\eta})}{\sum_{j=1}^{N} \sigma_j(\boldsymbol{v_a}, \boldsymbol{\eta})} \tag{38}$$

$$\sigma_i(\boldsymbol{v_a}, \boldsymbol{\eta}) = \begin{bmatrix} exp\left(-\dfrac{\|\boldsymbol{v_a} - \boldsymbol{c}_i\|}{b_i}\right) + \\ + exp\left(-\dfrac{\|\boldsymbol{\eta} - \boldsymbol{c}_i\|}{b_i}\right) \end{bmatrix} \tag{39}$$

In which $\boldsymbol{c}_i$is the central vector and $b_i \neq 0$. From equation (37), $\hat{\boldsymbol{\lambda}}(\boldsymbol{v_a}, \boldsymbol{\eta})$ is determined by:

$$\hat{\boldsymbol{\lambda}}(\boldsymbol{v_a}, \boldsymbol{\eta}) = \hat{\Re}^T \omega(\boldsymbol{v_a}, \boldsymbol{\eta}) \tag{40}$$

Utilising (38), the controller (36) becomes:

$$\hat{\boldsymbol{f}}_{\boldsymbol{a}} = \begin{pmatrix} \hat{\Re}^T \omega(\boldsymbol{v_a}, \boldsymbol{\eta}) - \dot{\boldsymbol{v}}_{\boldsymbol{ad}} \\ +\lambda_1(\boldsymbol{E}_3 + \boldsymbol{\Phi})^T \boldsymbol{J}_1^T \boldsymbol{A}^T \boldsymbol{J_1} \boldsymbol{P}^T \boldsymbol{s_1} \\ +\boldsymbol{K_1}\, tanh(\boldsymbol{z}_1) + \boldsymbol{K_2}|\boldsymbol{z}_1|^{2\beta-1} \end{pmatrix} \tag{41}$$

$$\hat{\boldsymbol{\tau}}_{\boldsymbol{a}} = -\boldsymbol{M}_a \hat{\boldsymbol{f}}_{\boldsymbol{a}}$$

The final mission is to find an online training rule $\hat{\Re}$ to achieve convergence in a short time interval.

Remark 5. The architecture of the utilised neural network in this paper is developed with a unique hidden layer that brings a possible scheme into reality and reduces the computational burden. During the system's operation, the neural network has to calculate the output before the change of states of the U-AUV system. That is the reason for the used network to be designed as in Figure 2.

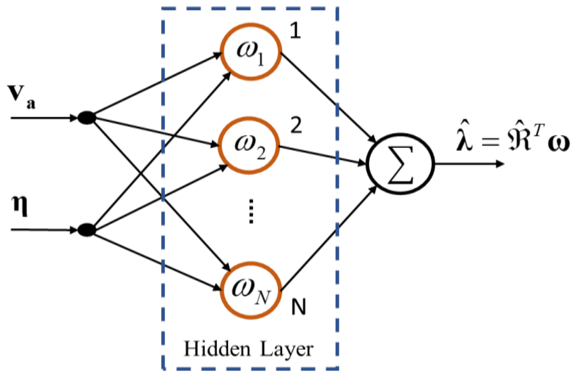

Figure 2. The structure of the utilised neural network.

3.3. Online training rule

To make $\hat{\Re} \to \Re$, using the third candidate Lyapunov function:

$$V_3 = \frac{\boldsymbol{s_1^T P s_1} + \boldsymbol{z_1^T z_1}}{2} + \frac{1}{2} tr\left(\tilde{\Re}^T \boldsymbol{\Lambda}^{-1} \tilde{\Re}\right) \quad (42)$$

Where $\tilde{\Re} = \Re - \hat{\Re}$ and $\boldsymbol{\Lambda}$ is an arbitrarily positive-define matrix. Differentiating from both sides of equation (40) yields:

$$\dot{V}_3 = \begin{pmatrix} \boldsymbol{\rho(s_1)} - \boldsymbol{K_1}|\boldsymbol{z}_1| - \boldsymbol{z}_1^T \boldsymbol{K_2} |\boldsymbol{z}_1|^{2\beta-1} \\ +\boldsymbol{z}_1^T \begin{pmatrix} \boldsymbol{M}_a^{-1} \boldsymbol{\hat{\tau}_a} + \Re^T \omega(\boldsymbol{v_a}, \boldsymbol{\eta}) - \boldsymbol{\dot{v}_{ad}} \\ +\lambda_1 (\boldsymbol{E}_3 + \boldsymbol{\Phi})^T \boldsymbol{J_1^T A^T J_1 P^T s_1} \\ +\boldsymbol{K_1} \tanh(\boldsymbol{z}_1) + \boldsymbol{K_2} |\boldsymbol{z}_1|^{2\beta-1} \end{pmatrix} \\ +\alpha_1 \lambda_{max}^{\boldsymbol{\Phi}^{-1}} \|\boldsymbol{\lambda_z}\|_F \left\|\tilde{\boldsymbol{\lambda}}_{\boldsymbol{z}}\right\|_{F_1}^T \end{pmatrix} - tr\left(\tilde{\Re}^T \boldsymbol{\Lambda}^{-1} \dot{\hat{\Re}}\right) \quad (43)$$

Substituting equation (39) into (41) and noting that $\boldsymbol{z}_1^T \Re^T \omega(\boldsymbol{v_a}, \boldsymbol{\eta}) = tr(\Re^T \omega(\boldsymbol{v_a}, \boldsymbol{\eta}) \boldsymbol{z}_1)$, we have:

$$\dot{V}_3 \le \begin{pmatrix} \boldsymbol{\rho(s_1)} - (\boldsymbol{K_1} + \|\zeta\|) \|\boldsymbol{z_1}\| \\ -\boldsymbol{z}_1^T \boldsymbol{K_2} |\boldsymbol{z}_1|^{2\beta-1} \\ +\alpha_1 \lambda_{max}^{\boldsymbol{\Phi}^{-1}} \|\boldsymbol{\lambda_z}\|_F \left\|\tilde{\boldsymbol{\lambda}}_{\boldsymbol{z}}\right\|_F \end{pmatrix} + tr\left(\tilde{\Re}^T \left(\omega(\boldsymbol{v_a}, \boldsymbol{\eta})(\boldsymbol{z}_1) - \boldsymbol{\Lambda}^{-1} \dot{\hat{\Re}}\right)\right) \quad (44)$$

From equation (42), the online training rule is designed as the following:

$$\dot{\hat{\Re}} = \boldsymbol{\Lambda} \omega(\boldsymbol{v_a}, \boldsymbol{\eta})(\boldsymbol{v_a} - \boldsymbol{v_{ad}}) - \alpha_2 \|\boldsymbol{z_1}\| \hat{\Re} \quad (45)$$

$$\boldsymbol{v_{ad}} = -\frac{1}{\lambda_1} \begin{bmatrix} (\boldsymbol{E}_3 + \boldsymbol{\Phi})^{-1} \boldsymbol{J_1^T A^{-1} J_1(\eta)} \times \\ \times \begin{pmatrix} \hat{\boldsymbol{\lambda}}_{\boldsymbol{z}} + \boldsymbol{\Xi^T s_1} + \boldsymbol{K_2} |\boldsymbol{s_1}|^{2\beta-1} \\ +\boldsymbol{K_1} \tanh(\boldsymbol{s_1}) \end{pmatrix} \end{bmatrix} \quad (46)$$

Where $\alpha_2$is a positive constant. Substituting equations (45) and (46) into (44) and using the Cauchy-Schwart inequation in the paper (Kim et al., 2023b) we have:

$$\dot{V}_3 \le \begin{pmatrix} \boldsymbol{\rho(s_1)} - (\boldsymbol{K_1} + \|\zeta\|) \|\boldsymbol{z_1}\| \\ -\boldsymbol{z}_1^T \boldsymbol{K_2} |\boldsymbol{z}_1|^{2\beta-1} + \alpha_1 \lambda_{max}^{\boldsymbol{\Phi}^{-1}} \|\boldsymbol{\lambda_z}\|_F \left\|\tilde{\boldsymbol{\lambda}}_{\boldsymbol{z}}\right\|_F \end{pmatrix} + \alpha_2 \|\boldsymbol{z_1}\| tr\left(\tilde{\Re}^T (\Re - \tilde{\Re})\right)$$

$$\le \begin{pmatrix} \boldsymbol{\rho(s_1)} - (\boldsymbol{K_1} + \|\zeta\|) \|\boldsymbol{z_1}\| + \boldsymbol{\Omega} - \\ \boldsymbol{z_1^T K_2} |\boldsymbol{z_1}|^{2\beta-1} - \alpha_2 \|\boldsymbol{z_1}\| \left\|\tilde{\Re}\right\|_F^2 \end{pmatrix} \quad (47)$$

In equation (47), $\Omega = \begin{pmatrix} \alpha_1 \lambda_{max}^{\boldsymbol{\Phi}^{-1}} \|\boldsymbol{\lambda_z}\|_F \left\|\tilde{\boldsymbol{\lambda}}_{\boldsymbol{z}}\right\|_F \\ +\alpha_2 \|\boldsymbol{z_1}\| \left\|\tilde{\Re}\right\|_F \|\Re\|_F \end{pmatrix}$. Since $0 < \beta < 1$, there always exists an invariant manifold $\partial(O)$ around the origin such that $\dot{V}_3 < 0$for all $\boldsymbol{z_1} \notin \partial(O)$ and $V_3$is bounded when $\boldsymbol{z_1} \in \partial(O)$. Therefore, this system is stable. The manifold is determined by:

$$\partial(O) = \left\{\boldsymbol{z_1} \in \mathbb{R}^3 \middle| \|\boldsymbol{z_1}\| < \frac{\alpha_2 \|\tilde{\Re}\|_F \|\Re\|_F}{\|\boldsymbol{K_2}\|}\right\} \quad (48)$$

Additionally, there exist three positive numbers a, b and $c$satisfying (Tung et al., 2023):

$$\dot{V}_3 \le -a\sqrt{V_3} - bV_3^{\beta} + c \quad (49)$$

According to the paper (Tung et al., 2023), with $0 < \kappa < 1$, Lyapunov function V_3 is bounded in a neighbourhood:

$$V_3 \le min\left\{\frac{1}{\sqrt{a}}\left(\frac{\delta}{1-\kappa}\right)^2, \sqrt[\beta]{\frac{\delta}{b(1-\kappa)}}\right\} \quad (50)$$

With the setting time $T_{max}$to be determined by"

$$T_{max} = \frac{2}{a\kappa} \frac{1}{b\kappa(\beta - 1)} \quad (51)$$

And the control scheme is shown in Figure 3.

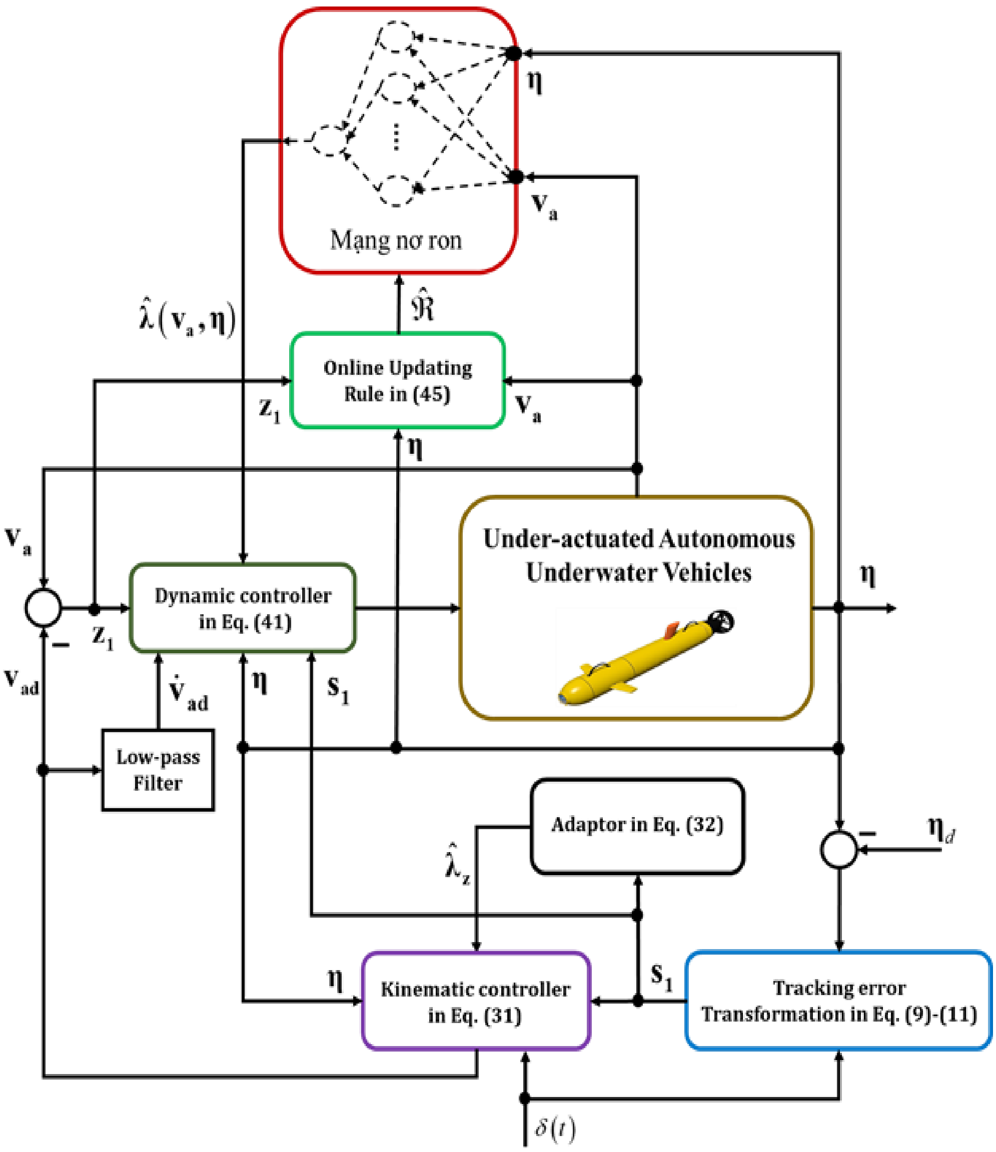

Figure (3). The control scheme of the closed-loop system.

4. Numerical Results

4.1. Initialisation

The proposed method is validated through simulation in this section and compared to the control-gaining-turning Backstepping (CGT Backstepping) method in (Chen et al., 2023) when the U-AUV's parameters are changed randomly during the whole simulation time. The model parameters of the un-actuated UAUV system are expressed by Li et al (2015) and they are listed in Table 1.

Table 1. The parameters of the UAUV system.

M	183	N_r	-160
I_{xx}	3	$X_{\dot{u}}$	-13
$I_{yy} = I_{zz}$	95	$Y_{\dot{v}}$	-257
I_{zz}	95	$Z_{\dot{w}}$	-257
X_u	-49	$N_{\dot{r}}$	-86
Y_v	-243	$M_{\dot{q}}$	-86
Z_w	-230	X_{uu}	-16
M_q	-140	Y_{vv}	-542
Z_{ww}	-62	M_{qq}	-62
N_{rr}	-78	g	9.81

The initial positions for the UAUV are selected as $14[m]$, $6[m]$ and $4[m]$ for $x(t)$, $y(t), z(t)$, respectively. The initial conditions for U-AUV's rotation angles are $\theta(0) = \psi(0) = 0[rad]$. The positive function $\delta(t) = \frac{1}{1+e^{-0.003t}}$ satisfying $\delta(t) > 0, \forall t$. The external disturbances that affect the closed-loop system are assumed to be time-varying and random functions with the range ± 200, representing the ocean fluid and hydraulic pressure. The desired trajectory is chosen as below:

$$x_d[m] = \begin{pmatrix} 10\,sin(\,0.06\,t) + \\ +10\,cos(\,0.03\,t) \end{pmatrix} \tag{52}$$

$$y_d[m] = \begin{pmatrix} 10\,sin(\,0.03\,t) + \\ +10\,cos(\,0.06\,t) \end{pmatrix} \tag{53}$$

$$z_d(m) = 200 \tag{54}$$

$$\boldsymbol{\eta_{1d}}(t) = [x_d \quad y_d \quad z_d]^T \tag{55}$$

The meaning of the desired trajectory shown in equations from (52) to (54) is that when the U-AUV achieves the desired depth, it will be stable at this depth and the trajectory is shaped by the desired tracking. The control parameters are selected as the following:

$$\boldsymbol{K}_1 = diag([0.3 \quad 0.3 \quad 0.2]) \tag{56}$$

$$\boldsymbol{K}_2 = diag([4 \quad 4 \quad 3]) \tag{57}$$

$$\alpha_1 = \alpha_2 = 0.1;\ \sigma = 4 \tag{58}$$

$$\boldsymbol{A} = 5\boldsymbol{E_3}, \boldsymbol{\Phi} = 5000\boldsymbol{E_3}, \boldsymbol{P} = \boldsymbol{E_3} \tag{59}$$

$$\lambda_1 = \lambda_2 = 1\ and \beta = \frac{13}{11} \tag{60}$$

In this simulation, M, I_{yy}, I_{zz} and $X_{\dot{u}}$ are assumed to be known, other parameters are unknown. The proposed controller does not use the model to perform, so the presentation of model's parameters is for simulation purpose only. According to the work (Chen et al., 2023), the limitation of the actuators able to supply is $\pm$ 700 (Nm). All the figures are simulated within 500 seconds.

Remark 6. It is essential to underscore again that the matrices $\boldsymbol{K_1}, \boldsymbol{K_2}, \boldsymbol{A}, \boldsymbol{\Phi}, \boldsymbol{P}$ should be positive-define, $\alpha_1, \alpha_2, \lambda_1, \lambda_2, \sigma$ and $\beta > 0{,}5$ to ensure the stability of the closed-loop system. However, $\|K_1\|$ should be small because it serves as the coeffident of tanh(.) whose signal are changed continuously when $v_a \to 0$, thereby reducing the undersired chatterring phenomenon. In constrast, $\|K_2\|$ should be large to accelerate the speed of states going to the origin. Additionally, ϕ should be large to reduce the maximum eigenvalues of ϕ^{-1}, thereby the term $\alpha_1 \lambda_{max}^{\boldsymbol{\Phi}^{-1}} \|\boldsymbol{\lambda_z}\|_F \|\tilde{\boldsymbol{\lambda}}_{\boldsymbol{z}}\|_F$ small enough not to affect the negative property of $\dot{V}_1$. This is also the reason for choosing small $\alpha_1 = \alpha_2 = 0{,}1 > 0$. The term β should not be too large to avoid the infinity number in simulation. That is the reason for choosing $\beta = \frac{13}{11}$.

4.2. Simulation results and discussion

This subsection is show the numerical results, compared to CGT Backstepping method.

Figure 4 shows the effectiveness of the proposed controller in this paper compared to the CGT Backstepping control of (Chen et al., 2023) in terms of the U-AUV's positions. Under conditions of uncertainly time-varying random parameters and external disturbances, the proposed model-free control steers $x, y, z$to track the desired point with a smaller error than the method in (Chen et al., 2023)

Figures 5 and 6 compare the performance of the proposed method with the CGT Backstepping method in controlling the system. In the first graph, the θ of the proposed method (red line) demonstrates significantly better stability than the CGT Backstepping method (blue line). The proposed method exhibits smaller oscillation amplitudes, particularly between 100 and 500 seconds, indicating less disturbance and a quicker convergence to a balanced state. In the second graph, the ψ of the proposed method (blue line) also shows superior performance. While both methods display a linear increase over time, the CGT Backstepping method (red line) suffers from larger oscillations. In contrast, the proposed method maintains greater stability throughout the 500-second duration, minimizing oscillations and ensuring smoother control. Overall, the proposed method outperforms the CGT Backstepping method in both pitch and yaw angles, achieving enhanced system stability and significantly reducing oscillations.

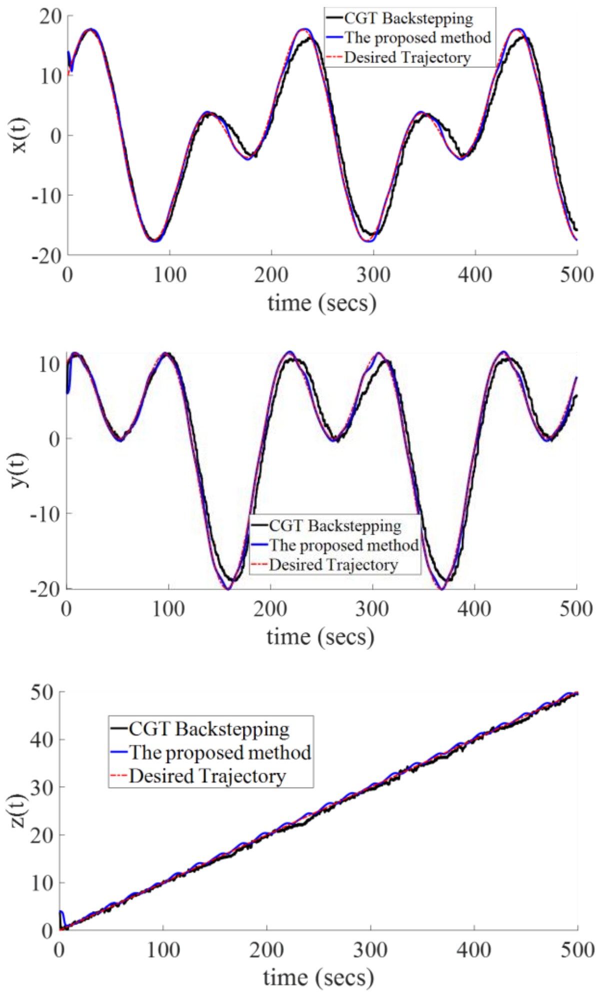

Figure 4. Positions of the studied U-AUV and their desired trajectory.

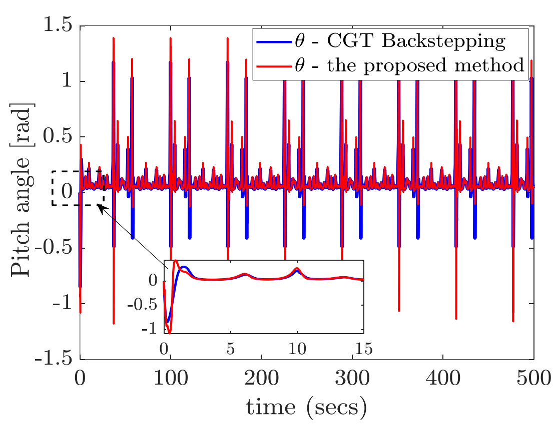

Figure 5. The UAUVs' Pitch angle.

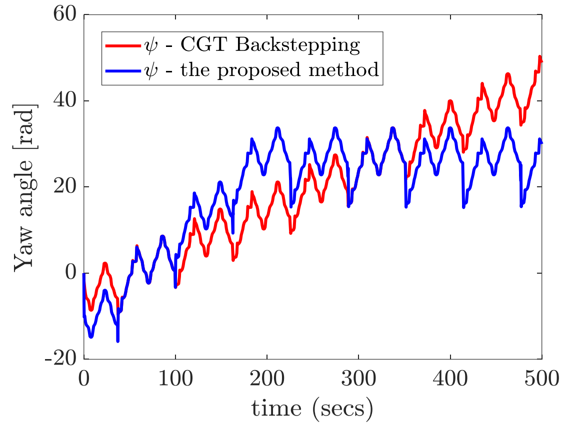

Figure 6. The UAUVs' Yaw angle.

Figure (7) shows the means of tracking errors regarding positions along x-,y-,z-axies where $M(e_m) = M(m_d - m)$ is symbolised for the means of errors with $m = x, y, z$. As can be seen in this figure, the means of errors of $x(t)$ and $z(t)$is significantly smaller than those of the CGT Backstepping method, nearly 1.5 for x and 0.3 for z. Means of errors in terms of $y$of our proposed method is a little higher than the compared method but not too much, only about 4.2 for the controller in this paper whereas the other method is 4.0.

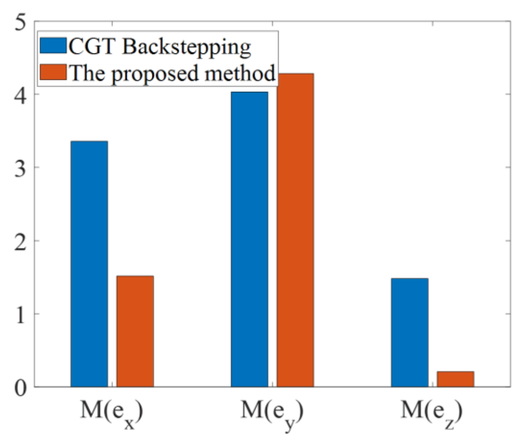

Figure 7. The mean of tracking errors.

Figure 8 illustrates the trajectory of the under-actuated AUV system with the proposed controller and the CGT Backstepping one. The trajectory, with the model-free controller, can track the desired trajectory in a short time interval regardless of the presence of external disturbances and randomly time-varying changes in UAUV's parameters, directly underscoring the effectiveness of the proposed method.

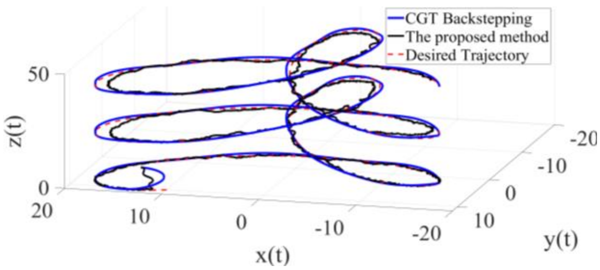

Figure 8. The trajectory of the under-actuated AUV.

In terms of the kinematic controller, Figure 9 shows the response of $\boldsymbol{z_1} = \boldsymbol{v_a} - \boldsymbol{v_{ad}} = [z_{11} \quad z_{12} \quad z_{13}]^T$. $\boldsymbol{z_1}$with the existing controller is more chaotic than the studied method. Since the proposed controller makes $\boldsymbol{z_1} \rightarrow \boldsymbol{0}$ while the CGT Backstepping only makes $\boldsymbol{z_1}$ to be bounded, the control performance of our method is better than the compared controller. The reason for these results is the CGT Backstepping method is only applied to the under-actuated AUV with a certain model. In the case of the uncertain model, control quality is not ensured. On the contrary, our method is developed under the assumption of an uncertain model. Thus, the control quality is better.

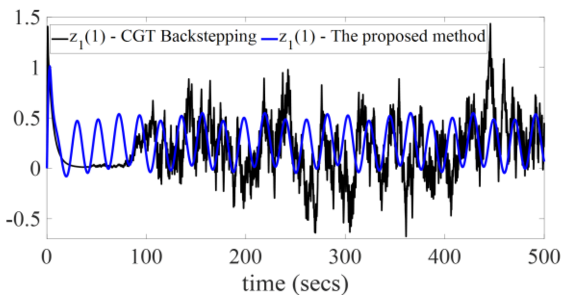

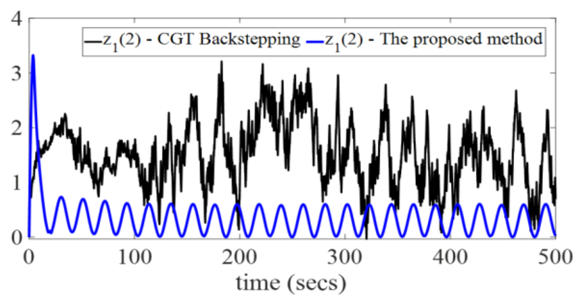

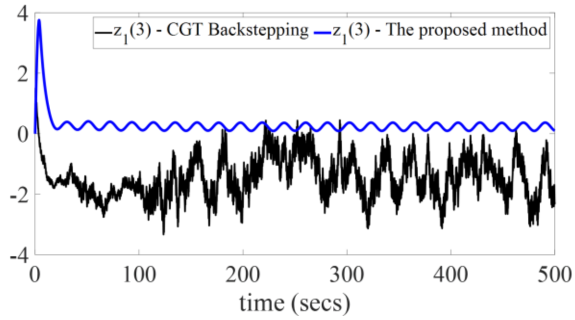

Figure 9. The error between $\boldsymbol{v_a}$ and $\boldsymbol{v_{ad}}$.

Table 2 shows some metrics of the tracking error $v_a - v_{ad}$, in which the pair of numbers (a,b,c) represents the metrics of $z_1(1), z_1(2)$ and $z_1(3)$, respectively. Clearly, the proposed method offers a lower percentage of overshoot value and lower means of $v_a - v_{ad}$.

Table 2. Metrics of the error ($\boldsymbol{v_a} - \boldsymbol{v_{ad}}$).

	CGT Backstepping	The proposed method
% overshoot value	(1.5, 3.1, -2.5)	(1.1, 3.3, 3.8)
The mean of ($\boldsymbol{v_a} - \boldsymbol{v_{ad}}$)	(0.22, 1.75, -1.84)	(0.25, 0.35, 0.08)
The level of fluatuation	high	low

The three charts compare the performance of two control methods, CGT Backstepping control and The proposed method, based on torque characteristics over time. The key observations are as follows: In the first chart, which illustrates the torque τ_u over time, the CGT Backstepping method exhibits significant overshoot with a peak value of approximately 1000 N during the initial phase. In contrast, the proposed method, while also displaying some initial oscillations, reaches a maximum value of around 800 N, demonstrating improved control. The proposed method rapidly suppresses oscillations and achieves stability within about 0.1 seconds, whereas the CGT Backstepping method requires a longer period to stabilize. The second figure of Figure 10, depicting torque τ_q, reveals that the proposed method has a notably higher initial overshoot, reaching a peak of approximately 300 Nm compared to about 150 Nm for the CGT Backstepping method. However, these oscillations in the proposed method quickly diminish, allowing the system to reach stability faster. In contrast, the CGT Backstepping method, despite its lower initial response, takes more time to completely eliminate oscillations.

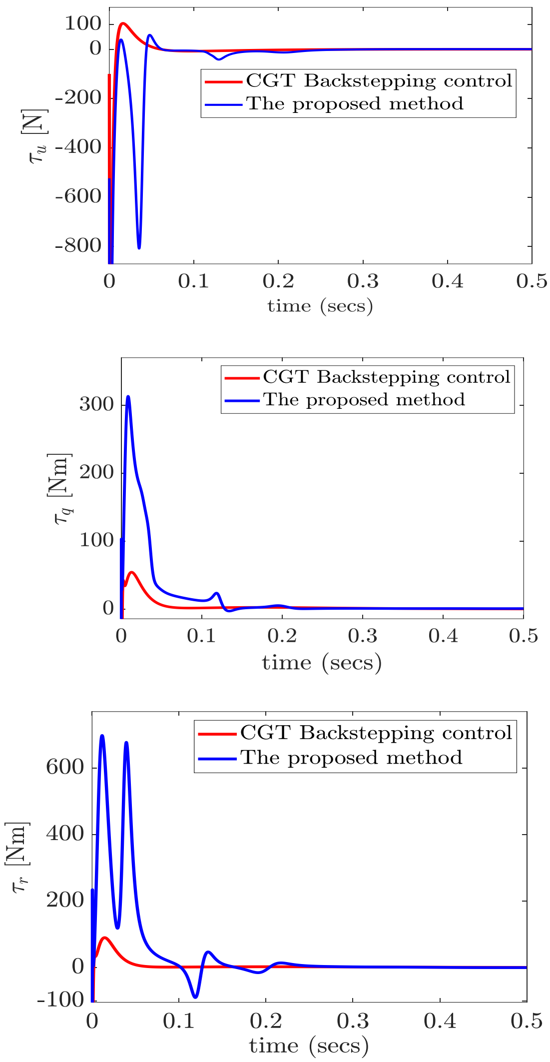

Figure 10. The input control signal of the proposed method.

The third figure of Figure 10, representing torque τ_r, highlights the most significant contrast between the two methods. While the CGT Backstepping method shows an initial overshoot of approximately 200 Nm, the proposed method exhibits a much larger peak of over 600 Nm. Nevertheless, the proposed method quickly reduces these oscillations and stabilizes in a shorter duration. On the other hand, the CGT Backstepping method, while more stable during the initial phase, requires more time to achieve full system stability. Overall, the proposed method demonstrates a clear advantage in achieving rapid stability, making it well-suited for applications requiring fast responses and high stability. However, its higher initial overshoot may be less desirable in scenarios demanding immediate stability, where the CGT Backstepping method provides a more consistent performance.

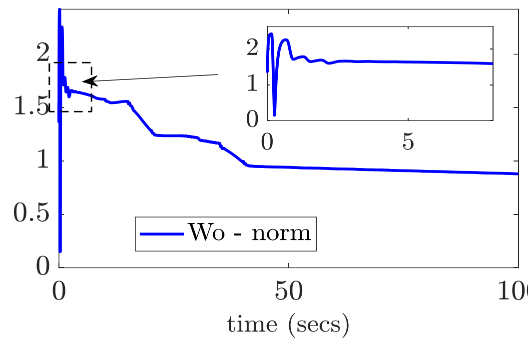

Figure 11. The evolution of neural network's weights over time.

Figure 11 depicts the evolution of $\|W\|$ over time, highlighting both its initial fluctuations and eventual stabilization. At the beginning, within the first 0 to 5 seconds, the value fluctuates around 2.0, as shown in the zoomed-in inset, indicating dynamic changes in the system before reaching stability. After this initial phase, the value begins to decrease gradually, following a nonlinear trajectory, and eventually converges to approximately 0.5 by the time it reaches 100 seconds. The graph illustrates a clear progression from an unstable initial state to a steady, stable condition, suggesting a process of optimization, energy dissipation, or system stabilization over time.

4.3. Limitations

In addition to the advantages of the model-free modified Backstepping-based controller that were demonstrated in previous sections, the disadvantages of the proposed controller are also mentioned. This method is an adaptive technique developed via training neural network; therefore, it clearly increases the computational burden compared to traditional methods such that active disturbance rejection (Shen et al., 2016) or sliding mode control (Qiao and Zhang, 2018). The computation-burden trade-off is unavoidable because it is essential to apply many advanced techniques to maintain control performance in the context of model uncertainties and unknown dynamics. Also, since utilising the state-of-the-art techniques to address uncertain dynamics, it directly amplifies the control input signal, leading to augmentation of the input signal's amplitudes (Figure 10). Thus, in the case of actuators that are only able to supply limited torque, it can be harmful for actuator systems.

Finally, although the tracking error is significantly reduced, a slight fluctuation exists (Figure 9) and mitigates the control quality. The application ability of this proposed method is also restricted when the system operates in a fast-disturbance environment, like a rapid-flowing water environment, because the network is not able to be trained in real time.

5. Conclusion and future work

This research presents a novel model-free, modified Backstepping controller for the 5-DoF under-actuated AUV system. A key contribution is the incorporation of an online-trained neural network, which ensures closed-loop stability in the presence of time-varying parameters. By comparing the proposed method with existing control approaches, we demonstrate significant improvements in tracking performance and robustness. The use of a control Lyapunov function not only guarantees the achievement of control objectives but also proves mathematical convergence. Numerical simulations show reduced tracking errors, enhancing both stability and adaptability. These advancements are vital for practical AUV applications, such as deep-sea exploration, where maintaining stability and precision in uncertain environments is critical.

In the future, a new deep learning approach and fuzzy logic system will built and used to regulate the under-actuated UAUV system to improve its resilience and adaptability when operating in an oceanic environment.

Acknowledgments

We would like to thank our colleagues in the Hanoi University of Mining and Geology for their supportive advice and meaningful contributions. Additionally, Dung Manh Do was funded by the Master Scholarship Programme of Vingroup Innovation Foundation (VINIF), code VINIF.2024.ThS.14.

Contributions of authors

Tung Thanh Sy Ngo - Conceptualization, Methodology, Writing draft & editing; Dung Manh Do - Software, Writing - review & editing, Methodology; Hai Xuan Le - Software, Writing - review & editing; Khoat Duc Nguyen - Methodology, Investigation.

References

An, S., Wang, L., & He, Y. (2022). Robust fixed-time tracking control for underactuated AUVs based on fixed-time disturbance observer. Ocean Engineering, 266, 112567.

Chen, H., Tang, G., Wang, S., Guo, W., & Huang, H. (2023). Adaptive fixed-time backstepping control for three-dimensional trajectory tracking of underactuated autonomous underwater vehicles. Ocean Engineering, 275, 114109.

Fossen, T. I. (1999). *Guidance and control of ocean vehicles*.

Kim, J., Joe, H., Yu, S. C., Lee, J. S., & Kim, M. (2015). Time-delay controller design for position control of autonomous underwater vehicle under disturbances. IEEE Transactions on Industrial Electronics, 63(2), 1052-1061.

Kim, T. D., Do, D. M., Hoang, D., Pham, T. N., Ha, M. H., & Le, H. X. (2023a). A Novel Separation Principle-Based Stabilization for 6-Dof Overhead Crane Under Fault Injection Data Onslaught. IEEE Access, 11, 102531-102549.

Kim, T. D., Nguyen, T., Manh Do, D., & Le, H. X. (2023b). Adaptive neural network hierarchical sliding mode control for six degrees of freedom overhead crane. *Asian Journal of Control*, *25*(4), 2736-2751.

Li, Y., Wei, C., Wu, Q., Chen, P., Jiang, Y., & Li, Y. (2015). Study of 3 dimension trajectory tracking of underactuated autonomous underwater vehicle. Ocean Engineering, 105, 270-274.

Luo, W., & Liu, S. (2023). Disturbance observer based nonsingular fast terminal sliding mode control of underactuated AUV. *Ocean Engineering*, *279*, 114553.

Qiao, L., & Zhang, W. (2018). Adaptive second-order fast nonsingular terminal sliding mode tracking control for fully actuated autonomous underwater vehicles. *IEEE Journal of Oceanic Engineering*, *44*(2), 363-385.

Shen, Y., Shao, K., Ren, W., & Liu, Y. (2016). Diving control of autonomous underwater vehicle based on improved active disturbance rejection control approach. Neurocomputing, 173, 1377-1385.

Song, R., Wei, Q., & Li, Q. (2019). *Adaptive dynamic programming: single and multiple controllers*. Singapore: Springer.

Tung, N. S. T., Dung, D. M., Hai, L. X., Minh, P. X., Khoat, N. D., & Quynh, H. D. (2023, December). A Finite-Time Recursion-Based Tracking Control for Under-Actuated Autonomous Underwater Vehicles. In *International Conference on Advances in Information and Communication Technology* (pp. 109-120). Cham: Springer Nature Switzerland.

Wang, X., Zhang, G., Sun, Y., Cao, J., Wan, L., Sheng, M., & Liu, Y. (2019). AUV near-wall-following control based on adaptive disturbance observer. *Ocean Engineering*, *190*, 106429.

Yang, H., & Ye, D. (2018). Adaptive fixed-time bipartite tracking consensus control for unknown nonlinear multi-agent systems: An information classification mechanism. Information Sciences, 459, 238-254.